Chalcogenide Letters Vol. 19, No. 12, December 2022, p. 955 - 964

Improved frictional properties of WS_2/TiO_2 composite layer in situ prepared on TC4 alloy

G. Y. Gu, J. Shang*, X. Y. Zhang
Liaoning University of Technology, Jinzhou, 121000, Liaoning Province, China

WS_2/TiO_2 composite layer was successfully in situ prepared by plasma electrolytic oxidation method adding Na_2S and Na_2WO_4 into electrolyte. The structure, morphology and frictional properties of the composite layer were investigated by X-ray diffraction, scanning electron microscopy, and 3D confocal microscopy. It was found that the WS_2/TiO_2 composite layer is denser and has a lower friction coefficient when the adding concentration is 10–20 g/L. The WS_2/TiO_2 composite layer in situ prepared by plasma electrolytic oxidation is a new method to improve the trilogical hehavior of TC4 alloy.

(Received September 2, 2022; Accepted December 15, 2022)

Keywords: Plasma electrolytic oxidation (PEO), Titanium alloy, WS_2/TiO_2 composite layer, In situ preparation

1. Introduction

Titanium alloys have advantages such as high strength and high specific strength due to their excellent bioconjugation properties [1,2]. However, considering the poor frictional properties of Ti-based materials [2,3], a need arises to improve the surface-layer properties through rational techniques. Means of surface modification such as physical/chemical vapor deposition, plasma spraying, ion implantation, laser melting (LSM/LST), sol-gel synthesis, surface metalizing, and electroplating are currently used to improve the tribological properties of Ti alloys.

Micro-arc oxidation (MAO), also known as plasma electrolytic oxidation (PEO), is a technique for modifying the surfaces of valve metals such as Ti [4–6]. Compared with previous treatment methods, MAO electrolyte loss is small, and it is reusable, with an easy-to-operate reaction at room temperature, and generates a rapid and uniform ceramic film. The resulting coatings show better corrosion resistance [7,8] and enhanced mechanical properties [9]. However, repeated breakdown, melting, and quenching during oxidation of the ceramic layer occur, thus forming inherent defects, such as microporosity and cracks [4,5,10] that require further enhancement of the oxide-layer properties. The surface morphology, porosity, layer composition, and layer thickness can be adjusted by changing the electrical and chemical process parameters [11,12].

Currently, in response to this need, the present research is focused on the of composite layers preparation by adding different particles in to electrolyte, such as Na_2Cu-EDTA [13]; Ag, Cu, and Zn [14]; K_2ZrF_6 [15]; $Cu_2P_2O_7$ [16]; and $Er(NO_3)_3$ [17], and the prepared composite layers

---

[*] Corresponding author: shangbahao@163.com

https://doi.org/10.15251/CL.2022.1912.955

couple some properties of the added particles on top of the original TiO_2 ceramic layer. The composite films were prepared by coupling several properties of the added particles, such as abrasion reduction, biological properties [18–21], and high hardness. The composite ceramic film layer generated by MAO in situ generation of additive particles has a strong bonding ability with the substrate and high hardness. Owing to the increase in surface hardness, the wear resistance of the surface is improved [22–28].

2. Experimental procedure

The TC4 sample was polished with sandpaper until its surface was free of obvious defects, and it was then ultrasonically cleaned for use. The electrical parameters were set to a constant current mode of 11 A/dm^2, a frequency of 500 Hz, and time of 30 min. Further, 2-g/L NaF+6-g/L Na_3PO_4+4-g/L Na_2WO_4 was used as the main salt system, and Na_2S was added at 10, 20, and 30 g/L as the control. The surface and cross-sectional morphologies of the prepared oxide films were observed using a Zeiss SIGMA 500 field-emission scanning electron microscope and an Aztec X-Max 50 energy spectrometer. The porosity was analyzed using Image J software with a D/max-2500/pc diffractometer with a Cu *Kα* target, a voltage and current of 40 kV and 100 mA, respectively, a scanning angle of 20°–90°, and a scanning speed of 8°/min.

3. Results and analysis

It was found from Fig. 1 that the surface morphology of the ceramic layer generated by MAO changes significantly with the increasing concentration of added Na_2S, and it can be seen that the pore diameter of the micro-pores distributed on the surface of the oxide layer fluctuates drastically up to 100 μm when the Na_2S concentration is low, while the pore diameter decreases to an average of 2–4 μm when the concentration reaches 30 g/L. Moreover, the pore-size distribution diagram shows that the pore size of the membrane layer decreases along with the porosity. However, the surface roughness of the oxide layer also improved significantly with increasing addition concentration. The roughness parameters in Fig. 2 are the following: R_a, arithmetic average roughness; R_p, maximum peak height; R_v, maximum valley height; R_z, average peak and valley depth; and R_q, root-mean-square roughness. The roughness of R_a, R_p, R_v, R_z, and R_q decreased with increasing Na_2S concentration, and the five parameters of oxide-layer roughness reached their lowest value, i.e., 30 g/L, simultaneously. The roughness is mainly determined by the degree of elevation of the discharge buildup and the degree of depression of the discharge micropores. Figure 3 shows that the porosity and thickness of the film layer have the same variation rule, i.e., it decreases with increasing added concentration, and the porosity of the film layer reaches a minimum of 15.4% compared with 42% at 10 g/L.

Regarding the porosity, pore size, and roughness, the reason that the film thickness has the same variation pattern is the effect of different additive concentrations on the voltage during the MAO process. In general, the roughness is mainly determined by the degree of elevation of the discharge buildup and the degree of depression of the discharge micropores. The discharge buildup has a significant influence. As can be seen in Fig. 4, the increase of Na_2S concentration has a significant effect on the reaction voltage during the oxidation process, with a decrease of approximately 100 V per 10 g/L of added Na_2S and a minimum reaction voltage of approximately 150 V at 30 g/L. The increase in Na_2S concentration leads to the flooding of the solution with a large number of S^{2-} ions, which reduces the conductivity of the solution, resulting in a decrease in reaction voltage. It has been shown that lower voltage carries less energy, and less molten oxide can be ejected from the substrate per unit time [29]; in addition, the pore size of the micro-pores left by the breakdown layer is small, which contributes to the uniform growth of the ceramic layer and improves the surface quality of the ceramic layer.

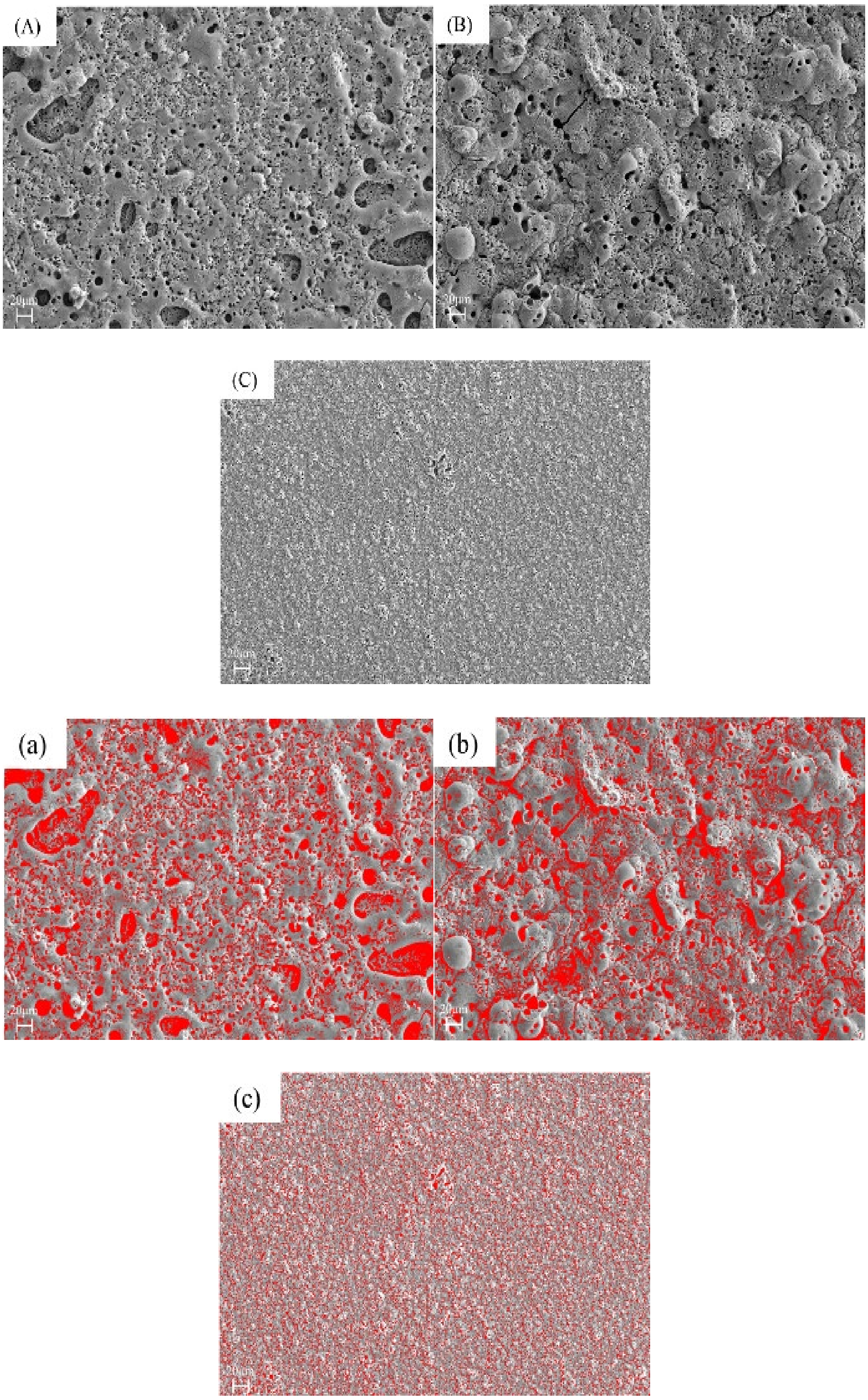

Fig. 1. Surface morphology and pore distribution of different Na_2WO_4 additions A, a 10g/L, B, b 20 g/L, C, c 30 g/L.

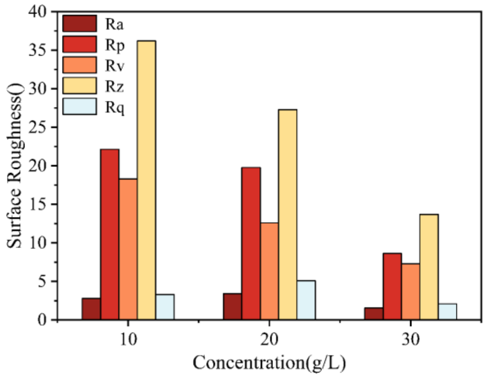

Fig. 2. Roughness of oxide layer with different Na_2WO_4 additions.

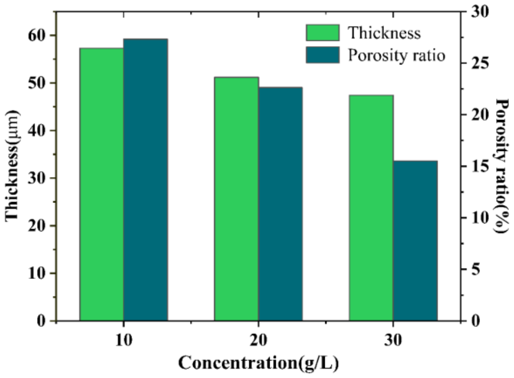

Fig. 3. Histogram of film thickness and porosity for different Na_2WO_4 additions

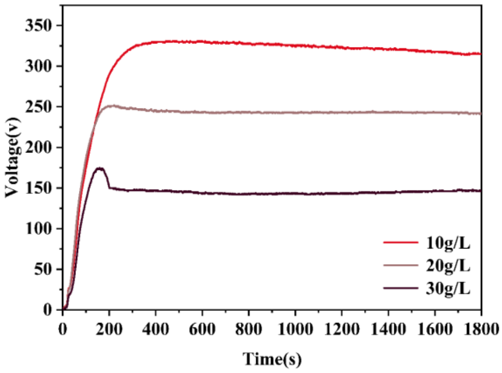

Fig. 4. Reaction voltage of different Na_2WO_4 additions.

After X-ray diffraction (XRD) of the composite oxide layer, Fig. 5 shows the XRD patterns of the composite ceramic layer from 20° to 90° in the range of 2θ. It can be seen that the main phases of the oxide layer are rutile-TiO_2 and anatase-TiO_2, and the diffraction peaks are enhanced around28°, which indicates that increased Na_2S content is beneficial to the generation of stable-phase rutile-TiO_2. Moreover, the WS_2 phase appears in the diffraction pattern, indicating that the WS_2 phase is successfully generated by the reaction between Na_2WO_4 and Na_2S during the

MAO process. The content and type of the oxide layers prepared with different concentrations of Na_2S were almost unchanged, indicating that Na_2S concentration did not change the phase composition of the ceramic layers. Figure 6 shows the composition of the ceramic layer after oxidation with different concentrations of Na_2S. As can be seen in Fig. 6, the oxide layer is mainly composed of elemental Ti, O, W, and S. O and Ti comprise the main elemental compositions in the ceramic layer, and Ti and O come from the surface TiO_2 phase, while the presence of elemental W and S indicates the generation of the WS_2 phase on the surface of the ceramic layer, which is consistent with XRD results.

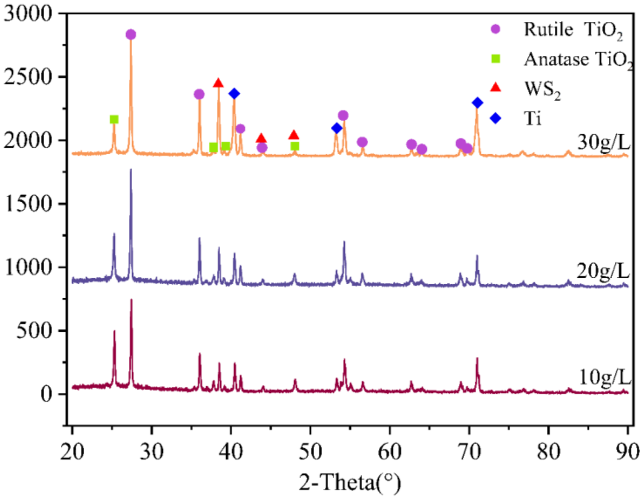

Fig. 5. X-ray diffraction of oxide layer with different Na_2WO_4 additions.

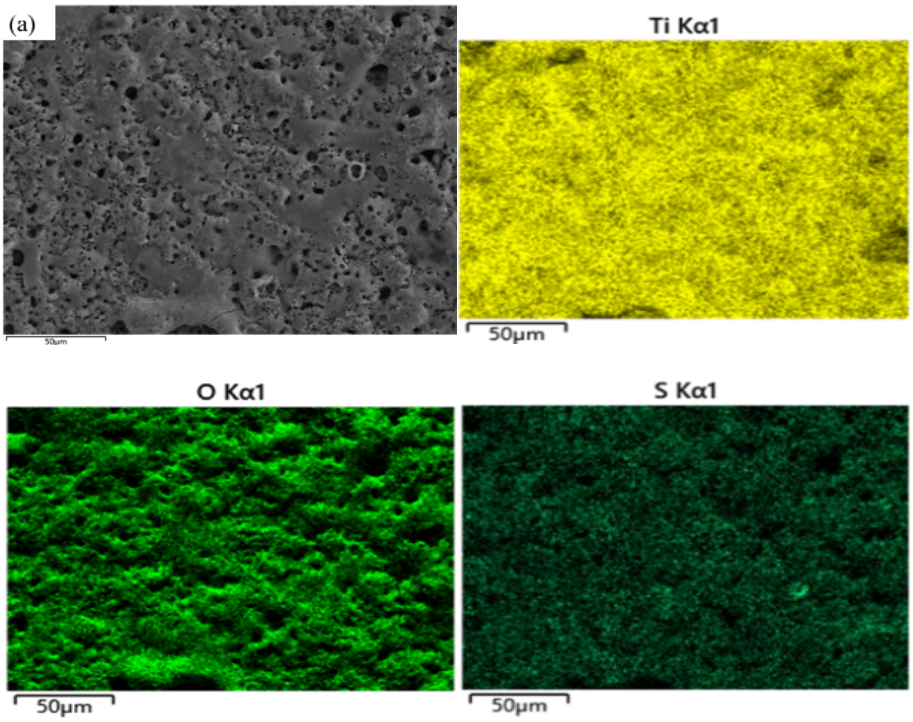

Fig. 6.1 SEM scans of the oxide layer with different Na_2WO_4 additions a) 10g/L,

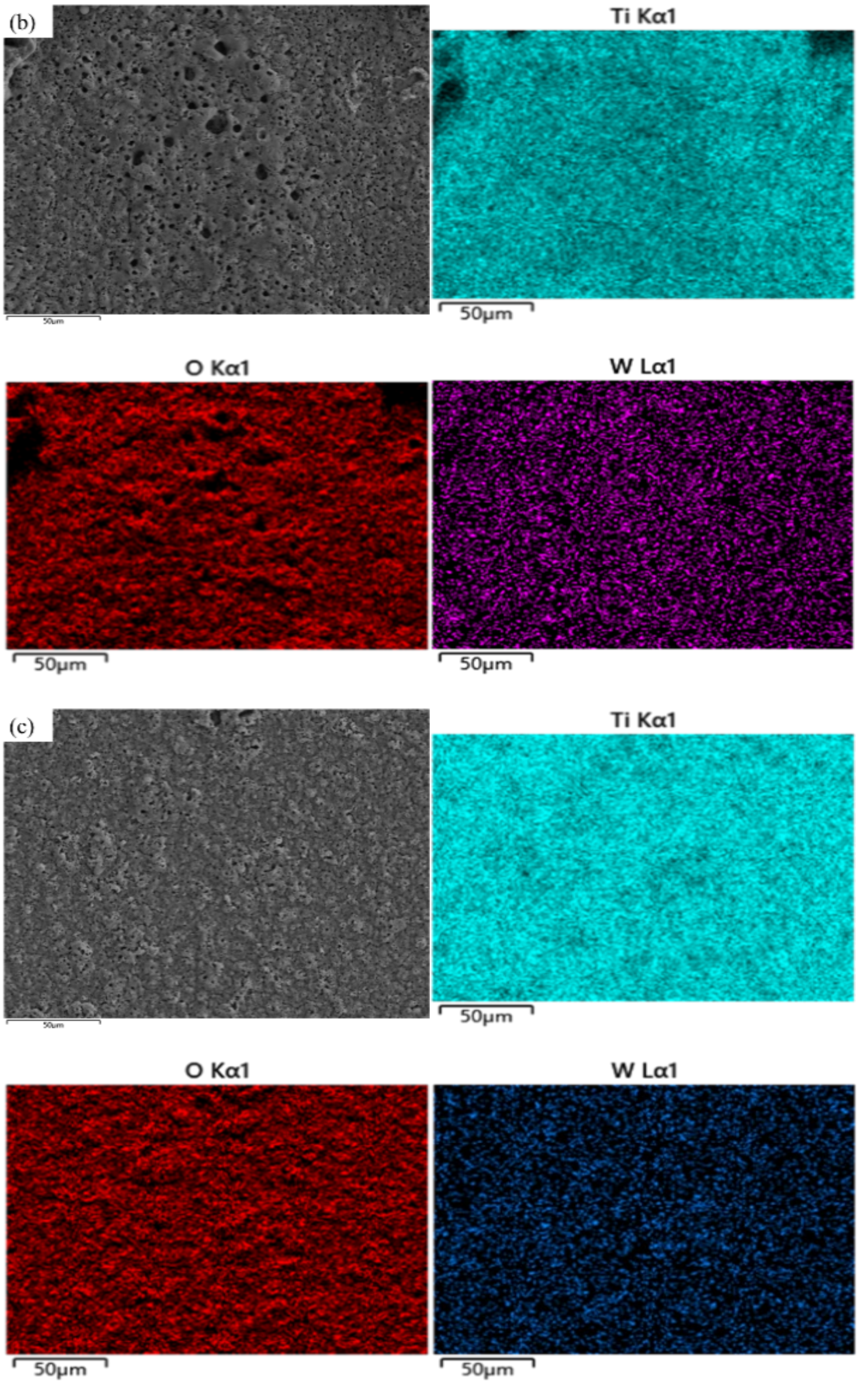

Fig. 6.2 SEM scans of the oxide layer with different Na_2WO_4 additions b) 20 g/L, c) 30 g/L.

The coefficient of friction (COF) of the coating prepared by the conventional PEO process is approximately 0.55 [30], and high-temperature friction experiments on the WS_2/TiO_2 composite coating revealed that the addition of Na_2S significantly reduced the average COF of the coating. As can be seen in Fig. 7, the COF of the coating gradually increased with the addition of Na_2S, but it was still smaller than the COF of the conventional coating. It can be seen from Fig. 8 that the COF of the coating stabilizes after 100 s, fluctuates slowly, and the COF curve is significantly higher than 10 g/L with the addition of 20 and 30 g/L or more of Na_2S. It can be concluded that the presence of WS_2 as a lubricating phase in the coating friction process provides a certain wear-reduction effect, while the COF increases with the addition of concentration probably because the large amount of S^{2-} ions in the electrolyte reduces the electrolytic properties of the solution, which reduces the reaction voltage and suppresses the COF of WS_2. Therefore, the addition of a high concentration of Na_2S reduces the wear resistance of the coating.

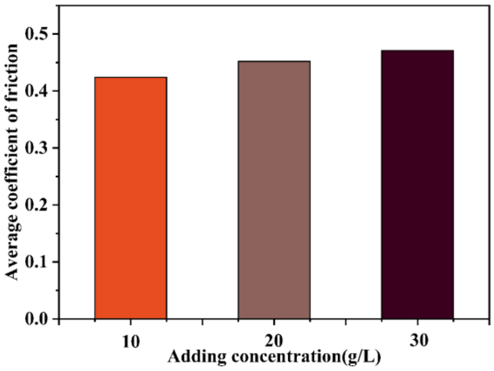

Fig. 7. Average friction coefficient of oxide layer with different Na_2WO_4 additions.

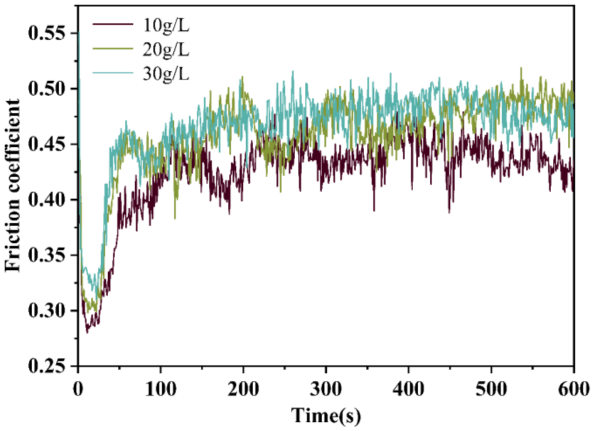

Fig. 8. Friction coefficient curve of oxide layer with different Na_2WO_4 additions.

Theoretically, the lattice mismatch between WS_2 and TiO_2 is large, and many dislocations and distortions exist at the interface, resulting in a non-coherent interface. The non-coherent interface may hinder the motion of dislocations, relieve lattice strain, and reduce the interfacial free energy [31], thereby producing moderate interfacial bond strength [32,33]. Thus, the non-coherent interfaces formed by the *in situ* synthesized WS_2 improve the mechanical properties of the ceramic coatings. As shown in Fig. 9, at the microscopic level, this non-coherent interface hinders the dislocation motion near the WS_2 nanoparticles, which allows WS_2 to be immobilized in the ceramic coating and ensures that WS_2 provides wear reduction for a long time.

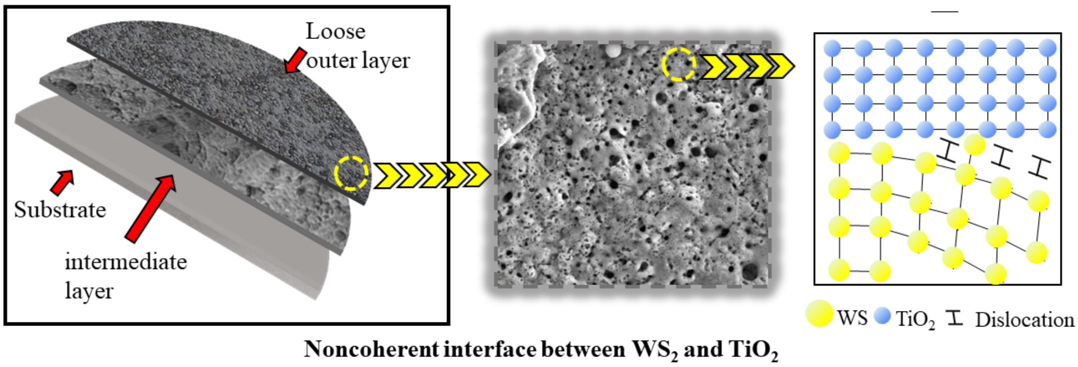

Fig. 9. Schematic diagram of the formation of non-coherent interface between WS_2 and TiO_2.

4. Conclusions

The following conclusions were drawn. The composite WS_2/TiO_2 layer can be *in situ* prepared by PEO treatment by adding Na_2WO_4 and Na_2S into the electrolyte. WS_2 plays a role in reducing wear to the layer, and the COF of the composite layer is lower than that of the conventional layer. The best addition concentration of Na_2S in the laboratory is 10–20 g/L.

References

[1] P. Jiang, Q. Wang, B.B. Zhang, Y. Wang, Chinese J. Eng. Des. 21(6) (2019) 95-101; https://doi.org/10.15302/J-SSCAE-2019.06.018
[2] R.R. Boyer, Mater. Sci. Eng. C. 213 (1996) 103-114; https://doi.org/10.1016/0921-5093(96)10233-1
[3] Y.M. Qi, Z.J. Peng, B.X. Liu, J. Liang, P. Wang, Surface Technology. 48(07) (2019)81-88; DOI:10.16490/j.cnki.issn.1001-3660.2019.07.008.
[4] A.L. Yerokhin, X. Nie, A. Leyland, A. Matthews, S.J. Dowey, Plasma electrolysis for surface engineering, Surf. Coat. Technol. 122 (1999) 73–93; https://doi.org/10.1016/S0257-8972(99)00441-7
[5] P.Gupta, G. Tenhundfeld, E.O. Daigle, D. Ryabkov, Surf. Coat. Technol. 201 (2007) 8746–8760. https://doi.org/10.1016/j.surfcoat.2006.11.023
[6] F.C. Walsh, C.T.J. Low, R.J.K. Wood, K.T. Stevens, J. Arcer, A.R. Poeton, A. Ryder, Trans. Inst. Met. Finish. 87 (2009) 122–135; https://doi.org/10.1179/174591908X372482
[7] S. Gowtham, T. Arunnellaiappan, N. Rameshbabu, Surf. Coat. Technol. 301 (2016) 63–73; https://doi.org/10.1016/j.surfcoat.2016.02.043
[8] M. Shokouhfar, C. Dehghanian, A. Baradaran, Appl. Surf. Sci. 257 (2011) 2617–2624; https://doi.org/10.1016/j.apsusc.2011.10.064
[9] S. Aliasghari, P. Skeldon, G.E. Thompson, Appl. Surf. Sci. 316 (2014) 463–476; https://doi.org/10.1016/j.apsusc.2014.08.037
[10] X.T. Shi, Y.Y. Zhu, S.F. Zhang, Materials Letters. 261: (2020) 126944; https://doi.org/10.1016/j.matlet.2019.126944

[11] O.A. Galvis, D. Quintero, J.G. Castaño, Surf. Coat. Technol. 269 (2015) 238-249; https://doi.org/10.1016/j.surfcoat.2015.02.036

[12] X.P. Lu, M. Mohedano, C. Blawert, Surf. Coat. Technol,307(2016) 1165-1182; https://doi.org/10.1016/j.surfcoat.2016.08.055

[13] X.X. Zhang, Z. Peng, X.Q. Lu, Y. Lv, G.Y. Cai, L. Yang, Z.H. Dong, Appl. Surf. Sci, 508(2020)144766; https://doi.org/10.1016/j.apsusc.2019.144766

[14]M.Shimabukuro,Antibiotics,,9(10)(2020)716;https://doi.org/10.3390/antibiotics9100716

[15] D. Li, L.H. Hua, K. Wen, X.C. Wang, Mater. Sci. Technol.211 (2022) 114493;

[16] J.P. Wei, W. Gao, Z.H. Cheng, Y.H. Jin, J. Chen, W. Yang, T Mater Heat Treat.42(03) (2021)162-167+184.

[17] Y.L. Zhang, Q.R. Li, G.J. Niu, C.H. Niu, C.H. Li, W.B. Li, J.Q. Pan, H.Y. Yi, X.L. Hao, R.X. Zhang, Chinese J. Anal. Chem.27(01) (2022) 9-17.

[18] J.Y. Ha, Y. Tsutsumi, H. Doi, Surf. Coat, 205 (21-22) (2011) 4948-4955; https://doi.org/10.1016/j.surfcoat.2011.04.079

[19] W.H. Song, H.S. Ryu, S.H. Hong, Antibacterial properties of Ag (or Pt)-containing calcium phosphate coatings formed by micro-arc oxidation[J]. Journal of Biomedical Materials Research Part A: An Official Journal of The Society for Biomaterials, The Japanese Society for Biomaterials, and The Australian Society for Biomaterials and the Korean Society for Biomaterials, 88 (1) (2009)246-254;https://doi.org/10.1002/jbm.a.31877

[20]L.H. Li, Y.M. Kong, H.W. Kim, Y.W. Kim, H.E. Kim, S.J.Heo, J.Y. Koak,Biomaterials, 25 (2004)2867-2875; https://doi.org/10.1016/j.biomaterials.2003.09.048

[21] J.Y. Suh, B.C. Jang, X.l. Zhu, J.L. Ong, K. Kim, Biomaterials,24(2) (2003) 347-355; https://doi.org/10.1016/S0142-9612(02)00325-3

[22] Y. Wang, B. Jiang, T. Lei, Mater. Lett.58(12-13) (2004) 1907-1911; https://doi.org/10.1016/j.matlet.2003.11.026

[23] E. Matykina, A. Berkani, P. Skeldon, Electrochim. 53(4) (2007) 1987-1994; https://doi.org/10.1016/j.electacta.2007.08.074

[24] Y. Yan, Y. Han, D. Li, Appl. Surf. Sci. 256(21) (2010) 6359-6366. https://doi.org/10.1016/j.apsusc.2010.04.017

[25] S. Durdu, M. Usta, Appl. Surf. Sci. 261 (2012) 774-782; https://doi.org/10.1016/j.apsusc.2012.08.099

[26] M. Babaei, C. Dehghanian, M. Vanaki, Appl. Surf. Sci. 357 (2015) 712-720; https://doi.org/10.1016/j.apsusc.2015.09.059

[27] Y. Cheng, J. Cao, M. Mao, Surf. Coat. 269 (2015) 74-82; https://doi.org/10.1016/j.surfcoat.2014.12.078

[28] R.O. Hussein, X. Nie, D.O. Northwood, Surf. Coat. 205(6) (2010) 1659-1667; https://doi.org/10.1016/j.surfcoat.2010.08.059

[29] B.J. Li, H. Zhao, X.H. Wang, Q. Z. Zhu, Journal of Shenyang Ligong University. 30 (03) (2011)59-61.

[30] J.M. Ríos, D. Quintero, J.G. Castaño, F. Echeverría, M.A. Gómez, Tribol Int. 128(2018)1-8; https://doi.org/10.1016/j.triboint.2018.07.010

[31] Z. Yang, Z. Zhang, Y. Chen, Scripta Materialia, 211 (2022) 114493; https://doi.org/10.1016/j.scriptamat.2021.114493

[32] D. Liu, A. Zhang, J. Jia, Compos. B. Eng., 212 (2021) 108681;

https://doi.org/10.1016/j.compositesb.2021.108681
[33] X. Han, P. Liu, D. Sun, Compos. B. Eng. 185 (2020) 107794.
https://doi.org/10.1016/j.compositesb.2020.107794